# Variability in FeB Pair Association Rates in Silicon under Ultrasound Loading: Effects of Acoustic Wave Types

OLIKH Oleg[1,a] and ARUTYUNOV Nikolay[,2,3,b]

[1]Department of General Physics, Taras Shevchenko National University of Kyiv, Kyiv, Ukraine

[2]Department of Physics, Martin Luther University Halle, Halle, Germany

[3]Leibniz-Institut für Kristallzüchtung (IKZ), Berlin, Germany

[a]olegolikh@knu.ua, [b]n_arutyunov@yahoo.com

**Keywords:** Ultrasound, Silicon, Iron-boron pair, Point defect, Acousto-defect interaction, Positron annihilation spectroscopy.

**Abstract.** Initially, this work briefly outlines how ultrasound can modify and characterize the defect system in semiconductors. Then, the study experimentally examines the effect of different types of acoustic waves on the association of FeB pairs in monocrystalline silicon. The results reveal that as the frequency of longitudinal waves increases, the ultrasound's effectiveness in accelerating the association rate decreases. Conversely, exciting transverse waves show the opposite trend. The study also assesses the potential to obtain a positron-annihilation response from the FeB complex in silicon, highlighting the advantages of conducting such measurements under ultrasound loading of the crystal.

## Introduction

Defects are well known to impact the properties of semiconductor devices significantly. In this regard, defect engineering, which involves controlled tuning of the defect-impurity subsystem to achieve new crystal, structure, or device properties, is crucial. One of the powerful tools for such active defect engineering is applying acoustic vibrations in the ultrasonic frequency range. For example, ultrasound treatment can stimulate the diffusion of various defects at temperatures close to room temperature due to the acoustically induced (AI) decrease in activation energy or over-barrier motion [1, 2]. Additionally, ultrasound (US) can cause the reconstruction of intrinsic point defects [3, 4, 5] or the annealing of radiation-induced defects [6, 7, 8]. Often, ultrasound serves not as the primary tool for modification but as an additional factor influencing the process during conventional technological operations, such as ion implantation [9, 10] or film deposition [11, 12].

In addition to the residual effects of ultrasound, acousto-dynamic effects also attract significant interest. In this case, changes in the state of defects and modifications to semiconductor properties are observed only under ultrasound loading (USL) conditions. After the cessation of acoustic wave (AW) propagation, the defect subsystem returns to its initial state, and the properties revert to their original condition. In particular, acousto-induced effects have been discovered, including changes in the configuration of metastable defects (FeB pairs and A-centers in Si [13, 14], EL2 in GaAs [15], DX in AlGaAs [16]), recharging of point defects (Te, vacancy, V-O in silicon structures [17, 18, 19], heterostructures GaAs/AlGaAs [20]), reconstruction of the Cottrell cloud (SiGe/Si, CdTe:Cl, CdHgTe [21, 22, 23]), and the formation of non-equilibrium dislocation clusters (GaP [24]). Such effects enable the creation of functional electronic devices, where control of the information signal relies on the inhomogeneities in the medium, which arise from the US action.

Acoustic waves also serve as a tool for characterizing the defect subsystem of semiconductors. For example, modifying elastic moduli during the formation of Jahn-Teller defects can cause extrema to appear in the temperature dependencies of US velocity and absorption. Such anomalies enable the successful investigation of intrinsic defects [25, 26] and substitutional atoms [27, 28] across various crystals. Another approach to US modification of traditional defect research methods involves acousto-dynamic effects. Specifically, while ultrasound propagates, the system's response to external

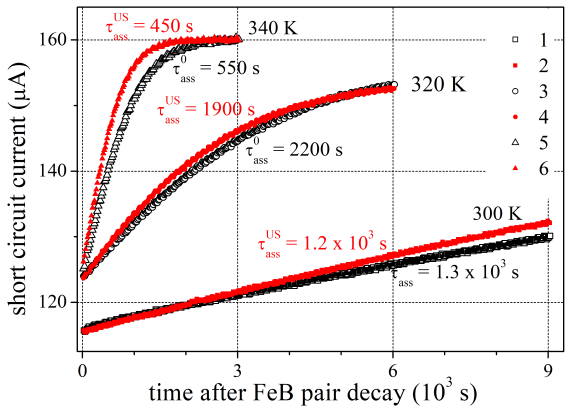


Fig. 1: Measured short circuit current plotted as a function of the time after FeB decay without USL (1, 3, 5, empty black marks) and under USL (2, 4, 6. filled red marks). $T$, K: 300 (1, 2), 320 (3, 4), 340 (5, 6). The values of $\tau_{\text{ass}}^{0}$ and $\tau_{\text{ass}}^{\text{US}}$ obtained by the methodology described in [34, 35] are shown also.

influences unrelated to elastic vibrations changes. It allows for obtaining more detailed information about defects than without AW. In particular, defect identification has been carried out using modified DLTS spectra, transmission and reflection measurements [29, 14, 30, 31].

This work examines the potential advantages of the acousto-positron perturbation technique, which involves conducting positron annihilation spectroscopy (PAS) under ultrasonic loading. The previously mentioned possible AI changes in the state of defects indicate that ultrasound can modulate the conventional PAS signal, including both positron annihilation lifetime spectroscopy (PALS) and coincidence Doppler broadening (CDB) spectroscopy (encompassing both high-momentum component W and low-momentum component S). Consequently, such studies could be more informative and, more importantly, may enhance the method's capabilities. For example, PAS is known to be most suitable for studying vacancy-type and acceptor-like defects [32]. The advantages of ultrasound as a defect engineering tool [18] may enable the expansion of the class of defects that can be studied using positron annihilation. In other words, the combination of PAS and ultrasound can provide new opportunities for studying defects in semiconductors, and this work aims to discuss the possibilities and prospects of this approach.

This study is focused on iron-related defects in Si:B. Iron is known to be one of the most detrimental metallic impurities in photovoltaic silicon. In $p$-type Si, iron atoms are predominantly bound into $\text{Fe}_i^+\text{B}_s^-$ pairs or occupy interstitial sites as $\text{Fe}_i^+$, forming defects that are traditionally difficult to study using PAS. The subsequent section presents experimental results that illustrate the variability in the effect of ultrasound on the defect subsystem. Specifically, it examines how vibrations with varying types influence the AI transformation processes between $\text{Fe}_i$ and FeB, which can occur readily at room temperature [33]. The penultimate section is devoted to quantitative estimates of positron annihilation in the FeB complex. Finally, the article concludes in the last section.

## Peculiarities of FeB Pair Association under Ultrasonic Loading Condition

**Experiment details.**The section

**Results of Acousto-induced Changes in Fe Ion Migration.**

## Positron Annihilation on FeB Complex: the Searching Estimations

The difference in both the size of atoms and their electron structure in FeB complex is the source of forming the strains and deformations in the crystal lattice of silicon. The thermalized positron has the excursion length [38] equal, approximately, to 1000 Å over the temperature range $\sim$ 25 to 300 K and thus may form a many-body electron-positron localized state at the FeB complex in case its concentration is not very much lower than about $10^{15}$–$10^{14}$ cm$^{-3}$. The rate of this localization ($k$) with the consequent emission of annihilation gamma-quanta out of the volume of FeB complex is determined by measuring the positron annihilation characteristics. The latter are known to be determined

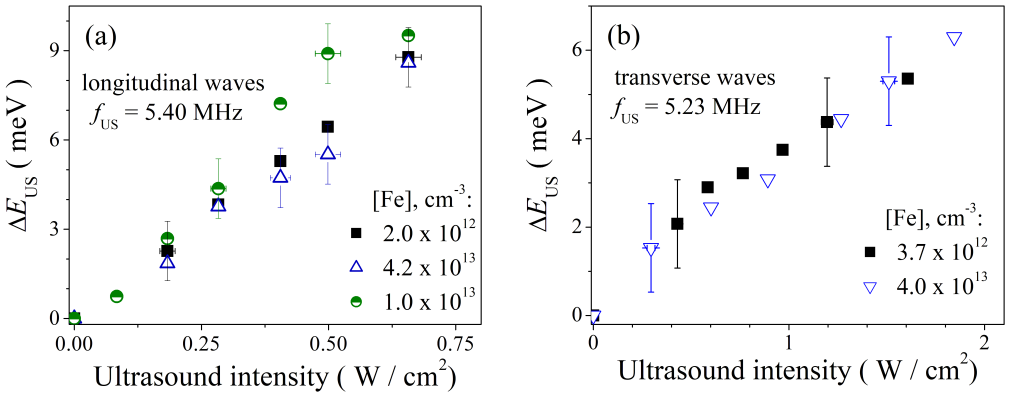


Fig. 2: Dependencies of AI change in migration energy on US intensity for samples with different iron concentrations. $f_{US}$, MHz: 5.40 (a), 5.23 (b). AW type: longitudinal (a), transverse (b). $T = 340$ K.

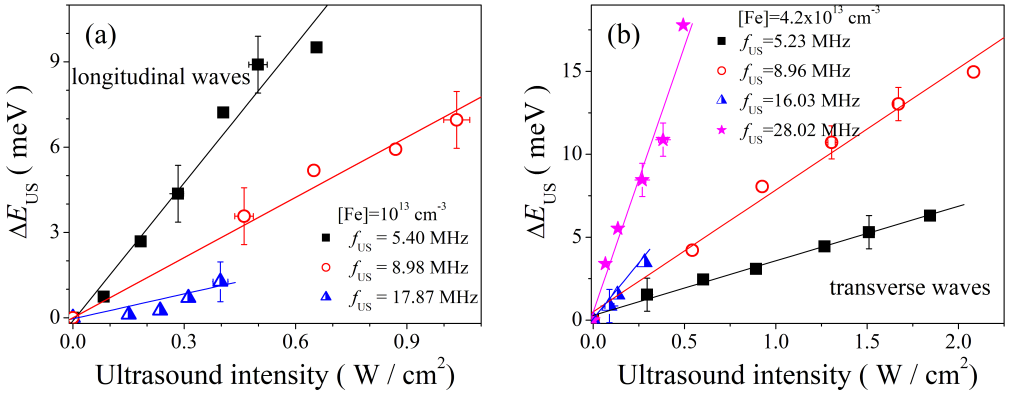


Fig. 3: Dependencies of AI change in migration energy on US intensity for various frequencies. [Fe], $10^{13}$ cm$^{-3}$: 1.0 (a), 4.2 (b). AW type: longitudinal (a), transverse (b). $T = 340$ K. The marks are experimental results, the lines are the linear fitted curves.

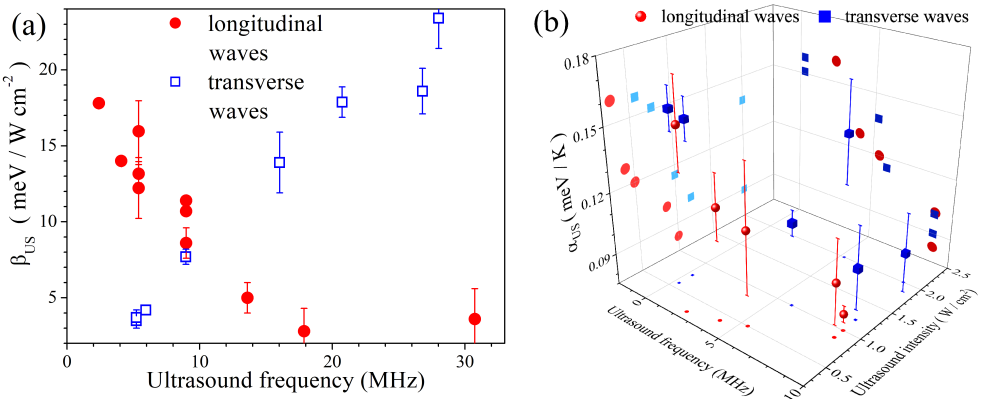


Fig. 4: Dependencies of intensity coefficient (a) and temperature coefficient (b) of AI changes on US frequency and intensity. $\beta_{US}$ values were obtained at $T = 340$ K. AW type: longitudinal (red circles), transverse (blue squares).

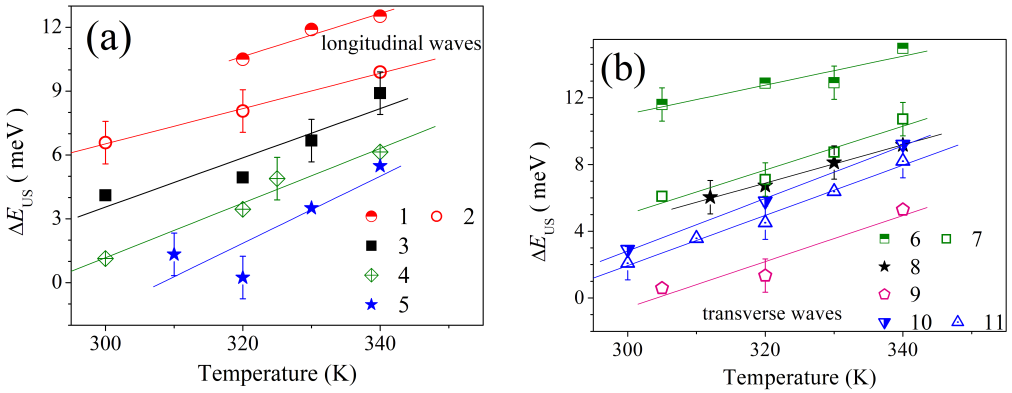


Fig. 5: Temperature dependencies of $\Delta E_{\text{US}}$. AW type: longitudinal (a), transverse (b). $f_{\text{US}}$, MHz: 8.98 (1, 2), 5.04 (3), 4.09 (4), 2.39 (5), 8.96 (6, 7), 5.94 (8), 5.23 (9), 0.31 (10, 11). $W_{\text{US}}$, W/cm$^2$: 1.0 (1, 8), 0.87 (2), 0.1 (3), 0.4 (4), 0.3 (5), 2.0 (6, 9), 1.2 (7), 0.76 (10), 0.58 (11). The marks are the experimental results, the lines are the linear fitted curves.

by both the open volume and chemical nature of atoms involved in a defect [38]. The positron probing of defects becomes indispensable when other methods (e. g., such as EPR and IR spectroscopy), are not informative ones. In addition, also one may point out to the NMR and acoustic nuclear magnetic resonance that are not used for studying nuclei having zero nuclear spin.

**Positron Trapping.** To detect acoustic loading on a defect by positron annihilation one needs to have positron states related to it. A propensity of the thermalized positron to be localized in the region of negative effective charge related to the impurity atoms of different nature together with the open volume of a defect is generally accepted to describe by the trapping model [39]:

$$k = \lambda_0 \frac{\eta}{1-\eta} \cong \lambda_0 \frac{\tau_{\text{av}} - \tau_0}{\tau_{\text{max}} - \tau_{\text{av}}}\,, \tag{1}$$

where the resulting probability of 2–gamma annihilation is measured assuming that the positron trapping rate $k$ allows one to determine conditional probability $\eta$ of the event of 2–gamma annihilation of $e^+e^-$ pair in the centers studied [39, 40]:

$$\eta = \frac{k}{\lambda_0 + k}\,. \tag{2}$$

The averaged positron lifetime $\tau_{\text{av}}$ is expected to depend on the acoustic loading, and $\tau_0$ is a positron lifetime out of a defect; this value is not measured. As $\tau_0$ magnitude it is generally accepted to use so-called $\tau_{\text{bulk}}$ value which is, e.g., determined experimentally for a defect–"free" material. The cross-section of positron localization with the subsequent 2–gamma annihilation $\sigma_+$ determines the $k$ value:

$$\sigma_+ = k/C\,, \tag{3}$$

where $C$ is the coefficient of localization of positron pair at the center [38]; $C = [\text{FeB}] \times v_+$ ($v_+$ is the velocity of positron on its excursion length $\sim (4\tau D_+)^{0.5}$ where $\tau$ and $D_+$ are the positron lifetime and the positron diffusion coefficient, respectively [38, 39]. Over the range of concentrations [FeB] from $2\times10^{13}$ cm$^{-3}$ to $\sim 10^{14}$ cm$^{-3}$ the $k$ value $k\{[FeB]; \sigma_+ = 10^{-12}\text{cm}^2\}$ increases from $\sim 0.5$ to $\sim 1$ ns$^{-1}$. In the case of increase of the positron trapping cross section up to $10{-}11$ cm$^2$ for the same range of concentrations of defects the value of the positron trapping rate increases from $\sim 2$ to $\sim 10$ ns$^{-1}$. This range of the $k$ magnitudes is well detected using both PALS and CDB.

The $k$ value may turn out to be more pronounced due to yet much larger values of cross-sections. It should be noted in this connection that large cross sections $\sim 3.32 \times 10^{-11}$ cm$^2$ and $\sim 10^{-10}$ cm$^2$ related to excitonic Auger capture of holes and multiphonon emission capture, respectively, have been reported for the FeB complex [41, 42].

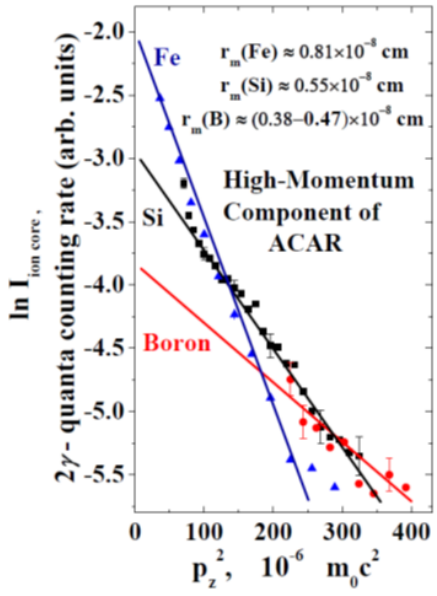


Fig. 6: The high-momentum component of the elementally-specific ACAR spectra obtained by the spectrometer of high geometrical angular resolution $\Delta \approx 0.48\times10^{-3}\, m_0\, c$ ($m_0$ and $c$ are the electron mass and the light velocity, respectively). The measurements were performed at room temperature and their results are given for boron (dots), silicon (squares), and iron (triangles). The electron-positron ionic radus $r_m$ were restored (see [43, 44, 45] for more detail). The lines are the results of fitting, the slopes of the linear functions are obtained with the accuracy which is characterized by the standard deviation / the Pearson's coefficient, respectively: 0.042/0.998 (Fe), 0.114/0.956 (B) and 0.101/0.99 (Si).
The many-body electron positron state at FeB complex modulated by USL must generate similar spectrum of high-momentum components of 2–gamma annihilation radiation.

Thus, one can expect observing the emission of annihilation radiation modulated by USL on FeB centers whose association was shown to be accelerated in the solar cells [35]. Special interest in this connection is a paradoxical divergence in the frequency dependency of reduced energy barrier for Fe ion migration when using longitudinal and transverse waves. This intriguing dependency observed suggests forming the anisotropic deformation field ambient FeB complex which consists of the atoms of Si, Fe, B and others, such as oxygen and carbon in Cz-grown silicon.

**Elementally-Specific Annihilation Radiation.** The ion cores of different chemical nature in the atomic environment of the positron makes the emission of the high-momentum annihilation gamma-quanta to be elementally specific one inasmuch as the wave functions of the ion core electrons retain to a great extent their atomic character in solids. The data obtained for these electron-positron states by the angular correlation of annihilation radiation (ACAR) of high resolution for the poly-crystalline metallic Fe (in its $\gamma$–phase), as well as for so-called $\beta$–B and dislocation-free $n$–type FZ–Si [111] single crystal are shown in Fig. 61. The electron-positron ion radii $r_m$ obtained by these data are close to the values of ionic radii $r_i$: for different coordination numbers $r_i(\mathrm{Fe}^{2+};\mathrm{Fe}^{3+})$ and $r_i(\mathrm{Si}^{4+})$ values range 0.63 to $0.92\times10^{-8}$ cm and 0.4 to $0.54\times10^{-8}$ cm, respectively; the ionic radius of boron $r_i(\mathrm{B}^{3+})$ is equal to $\simeq 0.27\times10^{-8}$ cm [46, 47]. The $r_m$(B) value is larger than the length of ionic radius $r_i(\mathrm{B}^{3+})$ as the maximum overlapping of the ion core electrons and positron wave functions [48] is shifted outwards the ion core of B atom more effectively than it takes place for ion cores of Fe and Si atoms.

The resulting emission of 2–gamma annihilation radiation out of Fe, Si, and B subvalent and ion core electron states to be probed with positrons follows the squares under the lines in Fig. 6. Similar trend should be observed for the many-body electron-positron state at FeB pair including its complexes with common impurities in Cz-Si. The relative contributions of these elementally-specific channels of annihilation radiation depend on the both configuration and symmetry of FeB complex, thus manifesting themselves in the mutually interrelated both the average positron lifetime, $\tau_{\mathrm{av}}$, and conditional probabilities, $\eta$; see Eq. 1 and Eq. 2. The numeral values of these parameters will be changed under USL, thus allowing one to observe the acoustic-positron annihilation phenomena. Instead of a high-precision ACAR measurements, the CDB may be used for detecting the electron-positron annihilation in the ion cores of atoms involved in the microstructure of defects, with the subsequent analysis of S-W-parameters of CDB spectra [38].

## Conclusion

## Acknowledgments

N. A. is thankful to DAAD for partial support of this work. O. O. is thankful to NRFU (Pr. No. 2023.03/0252) for partial financial support of this work.

## References

All manuscripts must be in English, also the table and figure texts, otherwise we cannot publish your paper.

Please keep a second copy of your manuscript in your office. When receiving the paper, we assume that the corresponding authors grant us the copyright to use the paper for the book or journal in question. Should authors use tables or figures from other Publications, they must ask the corresponding publishers to grant them the right to publish this material in their paper.

Use *italic* for emphasizing a word or phrase. Do not use boldface typing or capital letters except for section headings (cf. remarks on section headings, below).

## Organization of the Text

**Section Headings.** The section headings are in boldface capital and lowercase letters. Second level headings are typed as part of the succeeding paragraph (like the subsection heading of this paragraph).

**Page Numbers.** Do *not* number your paper:

**Tables.** Tables (refer with: Table 1, Table 2, ...) should be presented as part of the text, but in such a way as to avoid confusion with the text. A descriptive title should be placed above each table. Units in tables should be given in square brackets [meV]. If square brackets are not available, use curly {meV} or standard brackets (meV).

**Special Signs**. for example , $\alpha\ \gamma\ \mu\ \Omega\ ()\geq\pm\bullet\ \Gamma\ \{11\bar{2}0\}$ should always be written in with the fonts Times New Roman or Arial, especially also in the figures and tables.

**Macros**. Do not use any macros for the figures and tables. (We will not be able to convert such papers into our system)

**Language**. All text, figures and tables must be in English.

**Figures**. Figures (refer with: Fig. 1, Fig. 2, ...) also should be presented as part of the text, leaving enough space so that the caption will not be confused with the text. The caption should be self-contained and placed *below or beside* the figure. Generally, only original drawings or photographic reproductions are acceptable. Only very good photocopies are acceptable. Utmost care must be taken to *insert the figures in correct alignment with the text*. Half-tone pictures should be in the form of glossy prints. If possible, please include your figures as graphic images in the electronic version. For best quality the pictures should have a resolution of 300 dpi(dots per inch). Color figures are welcome for the online version of the journal. Generally, these figures will be reduced to black and white for the print version. The author should indicate on the checklist if he wishes to have them printed in full color and make the necessary payments in advance.

**Equations**. Equations (refer with: Eq. 1, Eq. 2, ...) should be indented 5 mm (0.2”). There should be one line of space above the equation and one line of space below it before the text continues. The equations have to be numbered sequentially, and the number put in parentheses at the right-hand edge of the text. Equations should be punctuated as if they were an ordinary part of the text. Punctuation appears after the equation but before the equation number, e.g.

$$c^2 = a^2 + b^2. \tag{4}$$

## Literature References

References are cited in the text just by square brackets [1]. (If square brackets are not available, slashes may be used instead, e.g. /2/.) Two or more references at a time may be put in one set of brackets [3,4]. The references are to be numbered in the order in which they are cited in the text and are to be listed at the end of the contribution under a heading *References*, see our example below.

## Summary

If you follow the ‘checklist‘ your paper will conform to the requirements of the publisher and facilitate a problem-free publication process.

## References


[1] S. Ostapenko: Appl. Phys. A: Mater. Sci. Process. Vol. 69 (1999), p. 225

[2] L.V. Borkovska, M.P. Baran, N.O. Korsunska et al.: Phys. B Condens. Matter Vol. 340–342 (2003), p. 258

[3] A. El-Bahar, S. Stolyarova, A. Chack et al.: Phys. Status Solidi A Vol. 197 (2003), p. 340

[4] U. Ritter, P. Scharff, V.V. Kozachenko et al.: Chem. Phys. Lett. Vol. 467 (2008), p. 77

[5] T. Wosinski, A. Makosa and Z. Witczak: Semicond. Sci. Technol. Vol. 9 (1994), p. 2047

[6] I. Ostrovskii, N. Ostrovskaya, O. Korotchenkov and J. Reidy: IEEE Trans. Nucl. Sci. Vol. 52 (2005), p. 3068

[7] A.M. Gorb, O.A. Korotchenkov, O.Ya. Olikh et al.: Solid-State Electron. Vol. 165 (2020), 107712

[8] A.M. Gorb, O.A. Korotchenkov, O.Ya Olikh and A.O. Podolian: IEEE Trans. Nucl. Sci. Vol. 57 (2010), p. 1632

[9] V. Litovchenko, V. Melnik and B. Romanjuk: Ukrainian Journal of Physics Vol. 60 (2015), p. 64

[10] B. Romanjuk, V. Kladko, V. Melnik et al.: Mater. Sci. Semicond. Process. Vol. 8 (2005), p. 171

[11] W. Wang, F. Huang, Y. Xia and A. Wang: J. Lumin. Vol. 128 (2008), p. 199

[12] S. Fujita, K. Kaneko, T. Ikenoue et al.: Phys. Status Solidi C. Vol. 11 (2014), p. 1225

[13] Ya.M. Olikh and M.D. Tymochko: Tech. Phys. Lett. Vol. 37 (2011), p. 37

[14] I. Ostrovskii, O. Korotchenkov, O. Olikh et al.: J. Opt. A: Pure Appl. Opt. Vol. 3 (2001), p. S82

[15] I.A. Buyanova, S.S. Ostapenko, A.U. Savchuk and M.K. Sheinkman: Mater. Sci. Forum Vol. 143 (1993), p. 1063

[16] A.E. Belyaev, H.J. von Bardeleben, M.L. Fille et al.: Mater. Sci. Forum Vol. 143 (1993), p. 1057

[17] O.A. Korotchenkov and H.G. Grimmliss: Phys. Rev. B. Vol. 52 (1995), p. 14598

[18] O.Ya. Olikh, A.M. Gorb, R.G. Chupryna and O.V. Pristay-Fenenkov: J. Appl. Phys. Vol. 123 (2018), 161573

[19] O. Olikh: Ultrasonics Vol. 56 (2015), p. 545

[20] B.N. Zaveryukhin, N.N. Zaveryukhina, R.A. Muminov and O.M. Tursunkulov: Tech. Phys. Lett. Vol. 28 (2002), p. 207

[21] V. Kuryliuk, A. Podolian and O. Korotchenkov: Cent. Eur. J. Phys. Vol. 8 (2009), p. 65

[22] Ya.M. Olikh and M.D. Tymochko: Superlattices Microstruct. Vol. 95 (2016), p. 78

[23] A.I. Vlasenko, Ya.M. Olikh and R.K. Savkina: Semiconductors Vol. 34 (2000), p. 644

[24] A.N. Gontaruk, D.V. Korbutyak, E.V. Korbut et al.: Tech. Phys. Lett. Vol. 24 (1999), p. 608

[25] K. Mitsumoto, M. Akatsu, S. Baba et al.: J. Phys. Soc. Jpn. Vol. 83 (2014), 034702

[26] M.Yu. Seyidov, R.A. Suleymanov, A.P. Odrinsky and C. Kırbas: Phys. B Condens. Matter Vol. 497 (2016), p. 86

[27] I.V. Zhevstovskikh, I.B. Bersuker, V.V. Gudkov et al.: J. Appl. Phys. Vol. 119 (2016), 225108

[28] J. Yi, H. Kong and C. Zhu: J. Alloys Compd. Vol. 474 (2009), p. 38

[29] O.A. Korotchenkov: Fizika i tekhnika poluprovodnikov Vol. 30 (1996), p. 1274

[30] I.V. Ostrovskii, O.A. Korotchenkov, R.M. Burbelo and H.G. Walther: Materials Science and Engineering: B Vol. 76 (2000), p. 139

[31] I.J. Fritz and T.M. Brennan: Semicond. Sci. Technol. Vol. 12 (1997), p. 19

[32] J. Slotte1, I. Makkonen and F. Tuomisto, in: Characterisation and Control of Defects in Semiconductors, edited by F. Tuomisto, volume 45 of Materials, Circuits and Devices, chapter, 6, Institution of Engineering & Technology (2019).

[33] C. Möller, T. Bartel, F. Gibaja and K. Lauer: J. Appl. Phys. Vol. 116 (2014), p. 024503

[34] O. Olikh, V. Kostylyov, V. Vlasiuk et al.: J. Appl. Phys. Vol. 130 (2021), 235703

[35] O. Olikh, V. Kostylyov, V. Vlasiuk et al.: J. Mater. Sci.: Mater. Electron. Vol. 33 (2022), p. 13133

[36] V.N. Pavlovich:Phys. Status Solidi B Vol. 180 (1993), p. 97

[37] V. Krevchik, R. Muminov and A. Yafasov: Phys. Status Solidi A Vol. 632 (1981), p. K159

[38] R. Krause-Rehberg and H.S. Leipner: *Positron Annihilation in Semiconductors* (Springer–Verlag, Berlin 1999).

[39] W. Brandt: Appl. Phys. Vol. 5 (1974), p. 1

[40] N. Arutyunov, M. Elsayed, R. Krause-Rehberg et al.: J. Phys. Condens. Matter Vol. 25 (2013), p. 035801

[41] B. Paudyal, K. Mcintosh and D. Macdonald, in: *Proceedings of the 34th IEEE Photovoltaic Specialists Conference (PVSC)*, IEEE (2009) p. 001588.

[42] A. Istratov, H. Hieslmair and E. Weber: Appl. Phys. A: Mater. Sci. Process. Vol. 69 (1999), p. 13

[43] N. Arutyunov, N. Bennett, N. Wight et al.: Phys. Status Solidi B Vol. 253 (2016), p. 2175

[44] N.Yu. Arutyunov and V.V. Emtsev: Mater. Sci. Semicond. Process. Vol. 9 (2006), p. 788

[45] N.Yu. Arutyunov and V.V. Emtsev: Mater. Sci. Semicond. Process. Vol. 11 (2008), p. 295

[46] J. Suchet: *Chemical Physics of Semiconductors* (Van Nostrand, N.Y. 1965).

[47] M. Rahm, R. Hoffmann, N. W. Ashcroft: Chem. Eur. J. Vol. 22 (2016), p. 1

[48] R. Ferrell:Rev. Mod. Phys. Vol. 28 (1956), p. 308